J Mater Sci: Mater Electron
DOI 10.1007/s10854-007-9481-4

Diffusion profiles and magnetic properties of Mn-implanted silicon after thermal annealing

Lee Chow · J. C. Gonzalez · E. Del Barco · R. Vanfleet · A. Misiuk · M. Prujszczyk · A. Shunmugavelu · G. Chai · J. Bak-Misiuk

Received: 28 September 2007 / Accepted: 6 November 2007
© Springer Science+Business Media, LLC 2007

Abstract Re-distribution of Mn atoms implanted into Czochralski silicon (CzSi:Mn) and floating zone silicon (FzSi:MN) after thermal annealing between 300 and 1,000 °C have been investigated by secondary ion mass spectroscopic technique. The motivation behind our study comes from recent report of strong magnetic ordering up to 400 K of Mn implanted silicon samples reported by Bolduc et al. (Phys Rev B 71:033302, 2005). Our silicon substrates were implanted with 160 keV Mn^+ ion to a dose of 1×10^{16} cm^{-2} at either room temperature or at 340 °C. The Mn profiles after annealing above 900 °C showed multiple concentration peaks for the 340 °C implanted samples, but not for the samples implanted at room temperature. We also carried out cross sectional TEM and ferromagnetic resonance measurements to correlate the micro-structural and magnetization data with the Mn depth profile obtained by SIMS.

L. Chow (✉) · J. C. Gonzalez · E. Del Barco
Department of Physics, University of Central Florida, Orlando, FL 32816, USA
e-mail: chow@ucf.edu

R. Vanfleet
Department of Physics, Brigham Young University, Provo, UT 84604, USA

A. Misiuk · M. Prujszczyk
Institute of Electron Technology, Al. Lotnikow 46, 02-668 Warsaw, Poland

A. Shunmugavelu
Mechnical, Materials, and Aerospace Engineering, UCF, Orlando, FL 32816, USA

G. Chai
Apollo Tech Inc., 205 Waymont Court, Suite 111, Lake Mary, FL 32746, USA

J. Bak-Misiuk
Institute of Physics, PAS, Al. Lotnikow 32/46, 02-668 Warsaw, Poland

1 Introduction

Bolduc et al. [1–3] recently reported ferromagnetism up to 400 K in both n-type and p-type silicon samples implanted with manganese, with ion doses 1×10^{15} and 1×10^{16} ions/cm^2. These results could have important implications on the development of dilute magnetic semiconductors [4, 5], which is an active research field. The ability to use ion implantation as a technique, and to use silicon as a substrate for the fabrication of dilute magnetic semiconductors has tremendous advantages over other techniques such at MBE [6, 7] or other materials such as III–V compound semiconductors [8, 9]. However, there are still debates and un-answered questions on the origin of this ferromagnetism in the Mn implanted silicon material. The main issue here is whether the magnetic ordering observed in Mn implanted silicon originated from “isolated” Mn ions in the substitutional sites (dilute magnetic materials), or from nano-clusters of Mn atoms or Mn silicides formed during the implantation or annealing stages. For instance, Zhou et al. [10] recently reported high resolution transmission electron microscopy (HRTEM) measurements on Mn-implanted silicon. They found that $MnSi_{1.7}$ nano-clusters were formed after rapid thermal annealing. While Verna et al. [11] studied the ferromagnetism in Mn ions implanted into Ge substrate, and did not observe the formation of extrinsic phases. We recently also investigated the effect of pressure annealing on the structure of Mn implanted silicon [12, 13] and the structure and

magnetic behavior of Cr and V implanted silicon materials [14, 15]. Here we report a careful investigation of the compositional, structural, and magnetic properties of Mn implanted silicon materials under different thermal annealing conditions.

2 Experimental

Mn^+ ions are implanted into Czochralski grown silicon at 340 °C (CzSi:Mn-1) and at room temperature (CzSi:Mn-2), and into floating zone silicon (FzSi:Mn-3) at 340 °C with a dosage of 1.0×10^{16} cm^{-2} and an energy of 160 keV. The CzSi is p-type with a carrier concentration of $N_p \approx 1 \times 10^{16}$ cm^{-3}, and oxygen concentration of $C_o \approx 9 \times 10^{17}$ cm^{-3}, (001) oriented, while the FzSi is n-type with a carrier concentration of $N_n \approx 1 \times 10^{14}$ cm^{-3} and an oxygen concentration of 1.5×10^{17} cm^{-3}. The annealing of the silicon samples was carried out in a Lindberg furnace under flowing Ar gas mixed with a minute amount of hydrogen. Details of the annealing procedure can be found in [16].

Secondary ion mass spectrometry was performed using a CAMECA IMS-3f magnetic sector analyzer. Details of the experimental procedures can be found in [16]. Transmission electron microscopy specimens were prepared in a cross sectional geometry by tripod polishing and viewed in a Tecnai TF20 in both TEM and STEM modes. Electron Energy Loss Spectroscopy (EELS) was used to identify the chemical composition of precipitates.

Ferromagnetic resonance measurements were conducted at room temperature by employing a broad-band (f = 1–40 GHz) coplanar waveguide (CPW) in the transmission mode as an inductive sensor and a 1.4 T electromagnet capable to rotate in a plane. The CPW is made of 300 nm thick gold deposited on an undoped GaAs substrate. The sample is placed upside-down on top of the central sensing area of the CPW to achieve the best coupling.

3 Results and discussion

3.1 Secondary ion mass spectrometry

In Fig. 1a–c, the diffusion profiles of CzSi:Mn-1 samples after anneal at different temperatures are shown. These samples were implanted at 340 °C and the warm implantation has caused a small concentration bump near

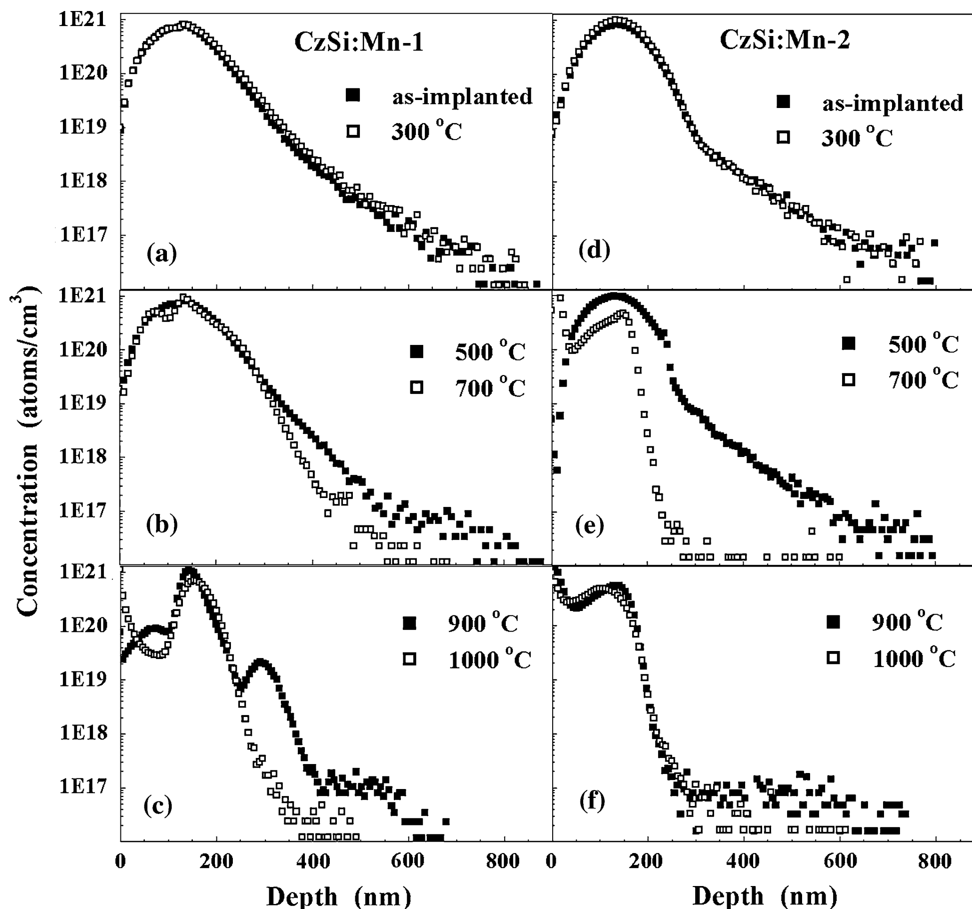

Fig. 1 Mn profiles of CzSi:Mn-1 (340 °C implantation) samples after thermal annealing at different temperatures, (**a–c**). Mn profiles of CzSi:Mn-2 (Room Temperature implantation) samples after thermal annealing at different temperatures, (**d–f**)

100 nm depth, which can be seen in Fig. 1a. This is apparently a unique feature for the warm implant. Another major feature in the warm implant is the tail portion of the Mn profile seems to extend into the silicon substrate more evenly. In Fig. 1a at a depth of 300 nm, there is no clear change in the slope, while for the room temperature implant (Fig. 1d), we can see there is a clear break of slope at about 300 nm. The 300 °C (Fig. 1a) and 500 °C (Fig. 1b) anneal did not seem to change the Mn profiles in any significant way. At 700 °C anneal, the concentration decrease in the tail portion (300 and 400 nm) seem to be related to getterring of manganese toward the EOR region at 250 nm, meanwhile there is a "minimum" in the Mn profile at 100 nm. This minimum is related to the concentration "bump" appeared in the as implanted sample. The Mn profile at 900 °C is the most intriguing one. We describe the profile as follow: between 300 and 400 nm, the concentration of Mn is relatively low and the Mn atoms seem to be gettered to the end-of-range region near 300 nm. The Mn profile has changed from one broad line into three peaks. The main peak located at 150 nm seems to be due to formation of nanoclusters. The other two minor profile peaks are located at 70 and 300 nm. The main peak at 150 nm seems to be quite stable even after the 1,000 °C annealed.

Figure 1d shows the Mn profiles of the CzSi:Mn-2 samples (Room Temperature implant) as implanted and annealed at 300 °C. We did not observe any profile modification due to 300 °C anneal. In Fig. 1e at 500 °C, the Solid Phase Epitaxial Regrowth (SPER) can be seen at a depth of 230 nm. At 700 °C anneal, the sweeping of Mn atoms through SPER seems to be very effective between 200 and 600 nm. But between the surface to 200 nm depth, Mn concentration remains to be very high. We will collaborate on this when discuss the TEM results. At 900 and 1,000 °C anneal (Fig. 1f), the Mn profiles remain similar to the 700 °C anneal.

In Fig. 2, the Mn profiles of FzSi:Mn-3 (340 °C implantation) samples are shown after annealing at different temperatures. We can see that the diffusion behavior of Mn and Mn profiles in FzSi:Mn-3 are quite similar to the CzSi:Mn-1 results. Both sets of samples were implanted at 340 °C. The signatures of warm implant are clearly seen here. It seems that the type of the silicon wafer has only very minor effects on the re-distribution of implanted Mn in silicon.

We note that in both warm implanted cases, we observed at certain depth (~150 nm), the concentration of Mn atoms actually increased rather than decreased. We attribute this to the precipitation of nano-clusters of Mn metal or Mn silicides that subsequently grow at the expense of lower concentration regions of the specimen.

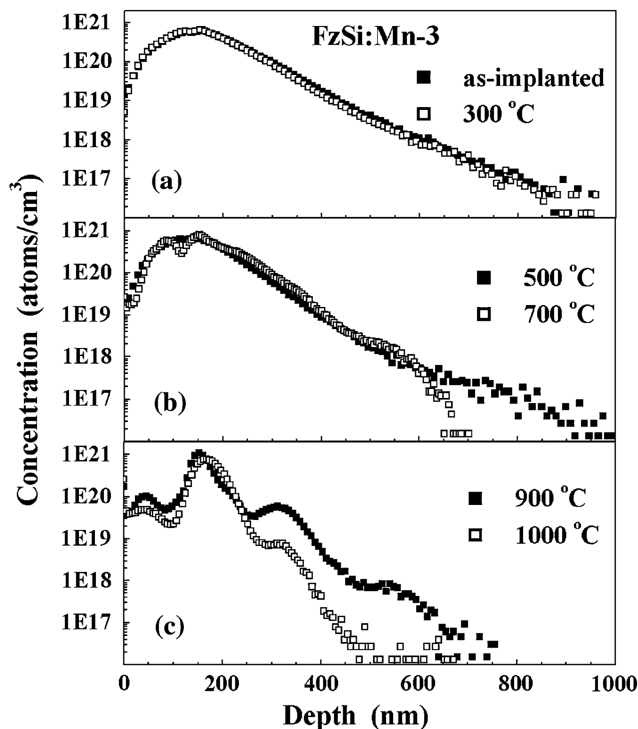

Fig. 2 Mn profiles of FzSi:Mn-3 (340 °C implantation) samples as-implanted and after 300 °C anneal (**a**), after 500 and 700 °C anneals (**b**), after 900 and 1,000 °C anneals (**c**)

3.2 Transmission electron microscopy

We have carried out extensive transmission electron microscopic work on these three sets of specimen. Details of these results (R. Vanfleet, unpublished data) will be published elsewhere. Here we present several typical results that reinforce our SIMS and FMR observations. In Fig. 3, the transmission electron micrographs of CzSi:Mn-2 annealed at 300, 500, and 700 °C are shown. The surfaces of the silicon substrates are lined up near the bottom of the figure. The scale bar at the bottom left of the figure is 200 nm. We can see the Mn implantation at 160 keV and 1×10^{16} cm^{-2} created an amorphous layer on the top surface of the silicon substrate. This layer is about 275 nm thick, with the typical "End of Range" (EOR) crystalline but damaged region below it. Small (~1 nm) precipitates of Mn can be seen in the amorphized layer. At 300 °C anneal, no significant movement of the a/c interface can be seen. At 500 °C anneal, solid phase epitaxial regrowth (SPER) has began with about 20 nm of regrowth and the Mn precipitates have grown to about 4 nm dimension. At 700 °C anneal, the solid phase epitaxial regrowth only progressed part way through the amorphized layer. The rest of the layer has crystallized into many mis-oriented grains. This is in direct contrast to previous results on Cr and V where SPEG progressed through the whole amorphized

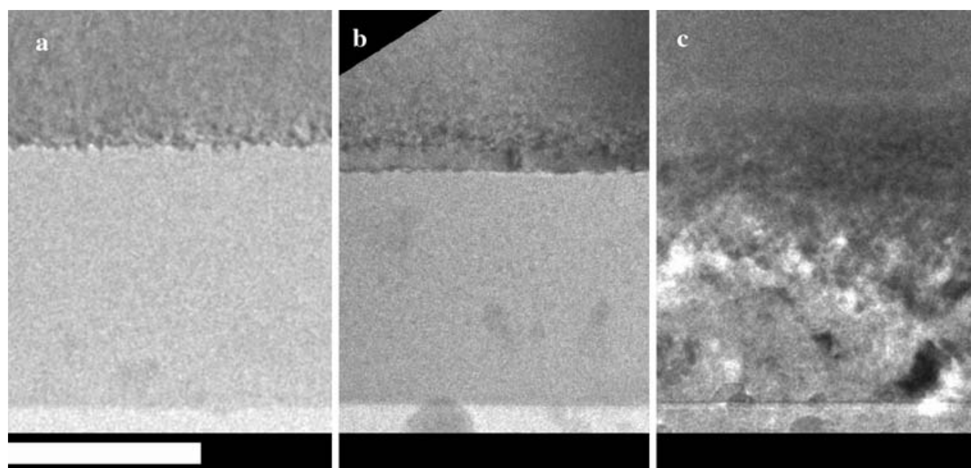

Fig. 3 Transmission electron micrographs of CzSi:Mn-2 annealed at (**a**) 300 °C, (**b**) 500 °C, and (**c**) 700 °C. The scale bar at bottom left is 200 nm

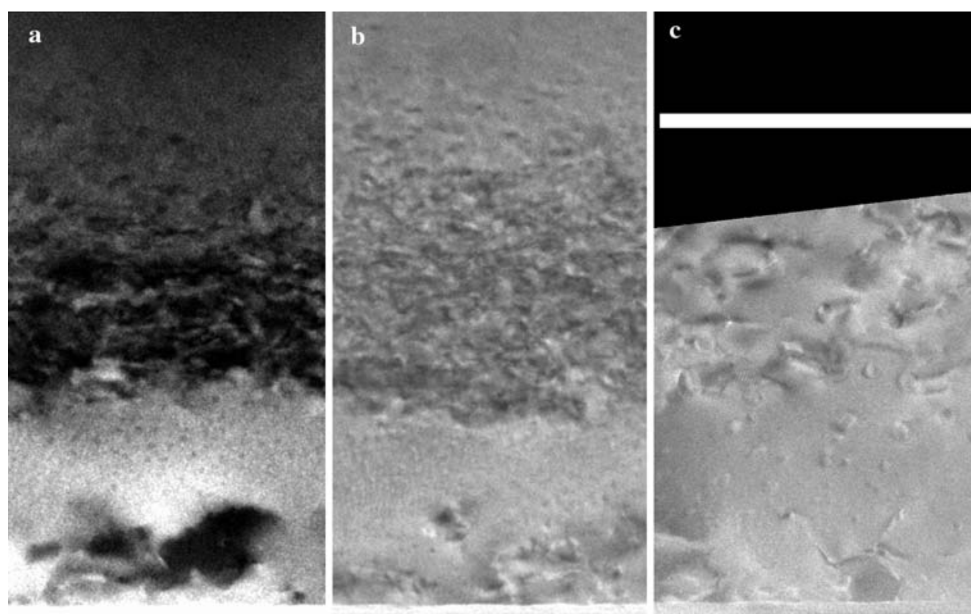

Fig. 4 Transmission electron cross sectional micrographs of CzSi:Mn-1 annealed at (**a**) 300 °C, (**b**) 500 °C, and (**c**) 700 °C. The scale bar at top right is 200 nm

layer. The peak Mn concentration and large Mn rich precipitates are seen in the transition region between epitaxial regrowth and polycrystalline silicon. Additionally, at the top surface of the specimen, large (30 nm) hemispherical Mn rich precipitates have formed.

In comparison, we also show in Fig. 4 the cross sectional TEM view of CzSi:Mn-1 (340 °C implantation) samples annealed at 300, 500 and 700 °C. The sample surface is at the bottom.

Here we can see that, since the implantation process took place at 340 °C, no amorphized layer is formed. The typical "End of Range" damage is still seen beginning at a depth of about 120 nm. There exists also a 50 nm region at the top surface where crystal defects (stacking faults and other dislocations) are seen. Mn-rich precipitates (2–4 nm in diameter) are seen between 50 and 300 nm in depth. Annealing to 700 °C results in precipitate growth with a region of small particle (5 nm diameter) between 40 and 110 nm in depth and a region of larger particles (6–12 nm in diameter) between 110 and 260 nm.

3.3 Ferromagnetic resonance spectroscopy

We carried out FMR measurements on the CzSi:Mn-1 sample that was annealed at 900 °C. A clear FMR signal is

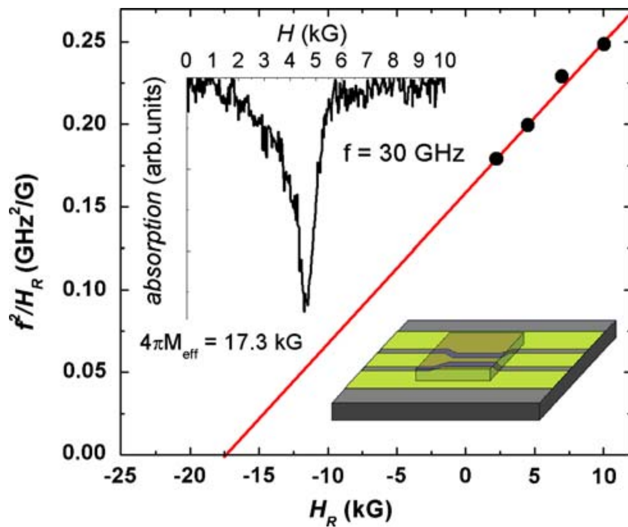

Fig. 5 Frequency dependence of the FMR resonance peak with the magnetic field applied in the plane of the substrate surface. The in-plane component of the Lande g-factor is g = 2.15. Assuming an isotropic film, a saturation magnetization of Ms = 1,350 emu/cm^3 is extracted from $4\pi M_{\mathrm{eff}}$. The insert shows a FMR spectrum recorded at f = 30.0 GHz. The sketch shows how the sample is placed upside-down on top of the CPW

observed in the absorption spectrum at 4.5 kG when the 30 GHz microwaves are employed (Fig. 5). At this frequency, the electron paramagnetic resonance (EPR) peak expected from isolated (i.e. paramagnetic) Mn-ions would be at $\approx$10 kG. Therefore, the observation of a peak at lower magnetic field indicates certain collective magnetic interaction between Mn ions and this resonance should be ascribed to dynamics of a rigid magnetic vector resulting from exchange coupling. When the magnetic field is applied in the plane of the substrate, the frequency dependency of the resonance field is expected [17] to follow a straight line when plotted as f^2/H vs. H, according to the in-plane FMR resonance condition,

$$\left(\frac{f}{2\pi\gamma}\right)^2 = H_{\mathrm{R}}(H_{\mathrm{R}} + 4\pi M_{\mathrm{eff}}) \quad (1)$$

Where the zero-field intercept gives $4\pi M_{\mathrm{eff}}$ (= $4\pi M_{\mathrm{s}}$ when there is no magnetic anisotropy) and the slope, which is the gyromagnetic ratio $\gamma = \frac{g\mu_{\mathrm{B}}}{\hbar}$, allows the determination of the Lande g-factor.

From our results, we obtained g = 2.15 and M_{eff} = 1,350 emu/cm^3. We have also carried out FMR experiments with the field applied at different angles with respect to the surface of the sample. The results (not shown) clearly indicate strong planar magnetostatic energy, indicative of an extended ferromagnetic film embedded inside the silicon. However, more experiments (i.e. as a function of dopant concentration) will be necessary to determine the extension of the exchange interaction within the film and to elucidate whether the sample is an extended ferromagnetic film or small planar ferromagnetic clusters are formed within the silicon substrate.

4 Summary

In summary, we have carried out detailed measurements using SIMS, TEM, and FMR to find out the origin of the ferromagnetism observed in Mn^+ ions implanted silicon. Our SIMS measurements show that after annealing, the concentration of Mn can increase in the depth of the substrate. The TEM measurements confirm the SIMS results and showed clearly formation of Mn metal or Mn silicides nanoclusters. The size of these nano-clusters depends on the annealing temperatures and can range from ~1.0 nm to more than 5 nm. The ferromagnetic resonances measured could very likely come from the magnetic interaction between these magnetic nano-clusters. Future experiments on the temperature dependence of FMR are planned.

Acknowledgments L. Chow acknowledges partial financial support from Apollo Tech, Inc. and Florida High Tech Corridor Program.

References

1. M. Bolduc, C. Awo-Affouda, A. Stollenwerk, M.B. Huang, F.G. Ramos, G. Abnello, V.P. LaBella, Phys. Rev. B **71**, 033302 (2005)
2. M. Bolduc, C. Awo-Affouda, F. Ramos, V.P. LaBella, J. Vac. Sci. Technol. A **24**(4), 1648 (2006)
3. M. Bolduc, C. Awo-Affouda, A. Stollenwerk, M.B. Huang, F.G. Ramos, G. Abnello, V.P. LaBella, Nucl. Instrum. Methods Phys. Res. B **242**, 367 (2005)
4. H. Ohno, Science **281**, 951 (1998)
5. S.A. Wolf, D.D. Awschalom, R.A. Buhrman, J.M. Daughton, S. von Molnar, M.L. Roukes, A.Y. Chtchelkanova, D.M. Treger, Science **294**, 1884 (2001)
6. H. Ohno, A. Shen, F. Matsukura, A. Oiwa, A. Endo, S. Katsumoto, Y. Iye, Appl. Phys. Lett. **69**, 363 (1996)
7. R.K. Singh, S.Y. Wu, H.X. Liu, L. Gu, D.J. Smith, N. Newman, Appl. Phys. Lett. **86**, 012504 (2005)
8. N. Theodoropoulou, A.F. Hebard, M.E. Overberg, C.R. Abernathy, S.J. Pearton, S.N.G. Chu, R.G. Wilson, Appl. Phys. Lett. **78**, 3475 (2001)
9. N. Theodoropoulou, A.F. Hebard, S.N.G. Chu, M.E. Overberg, C.R. Abernathy, S.J. Pearton, R.G. Wilson, J.M. Zavada, J. Appl. Phys. **91**, 7499 (2002)
10. S. Zhou, K. Potzger, G. Zhang, A. Mucklich, F. Eichhorn, N. Schell, R. Grotzschel, B. Schmidt, W. Skorupa, M. Helm, J. Fassbender, D. Geiger, Phys. Rev. B **75**, 085203 (2007)
11. A. Verna, L. Ottaviano, M. Passacantando, S. Santucci, P. Picozzi, F. D'Orazio, M. De Biase, R. Gunnella, M. Berti, A. Gasparotto, G. Impellizzeri, F. Priolo, Phys. Rev. B **74**, 085204 (2006)
12. A. Misiuk, J. Bak-Misiuk, B. Surma, W. Osinniy, M. Szot, T. Story, J. Jagielski, J. Alloys Comp. **423**, 201 (2006)
13. A. Misiuk, B. Surma, J. Bak-Misiuk, A. Barcz, W. Jung, W. Osinniy, A. Shalimov, Mater. Sci. Semicond. Process **9**, 270 (2006)

14. A. Misiuk, L. Chow, A. Barcz, B. Surma, J. Bak-Misiuk, P. Romanowski, W. Osinniy, F. Salman, G. Chai, M. Prujszczyk, A. Trojan, in *High Purity Silicon 9*, ed. by C.L. Claeys, R. Falster, M. Watanabe, P. Stallhofer (Pennington, 2006), p. 481
15. A. Misiuk, A. Barcz, L. Chow, B. Surma. Submitted to Solid State Phenomena
16. H. Francois-Saint-Cyr, E. Anoshkina, F. Stevie, L. Chow, K. Richardson, D. Zhou, J. Vac. Sci. Technol. B **19**, 1769 (2001)
17. C. Kittel, *Introduction to Solid State Physics*, 7th ed. (Wiley, New York, 1996)